Principles and Implementation of a Novel Radial-Anti-Disturbance Bearingless Switched Reluctance Motor

YUNHONG ZHOU[ID], JIAHAO JIANG, YUKUN SUN, AND PAN HU

School of Electrical Power Engineering, Nanjing Institute of Technology, Nanjing 211167, China

Corresponding author: Yunhong Zhou (zyh@njit.edu.cn)

ABSTRACT In order to solve the problem that the vehicle flywheel battery is easy to be disturbed in the process of using, a novel radial-anti-disturbance bearingless switched reluctance motor (RADBSRM) is proposed and studied based on the double stator switched reluctance motor. By widening the width of rotor poles, the flat top regions of all main winding inductances for each phase are constructed. By adopting the two-phase-conducting decoupling control rules, the electromagnetic torque and the main levitation force can be provided simultaneously. The auxiliary windings and the permanent magnet comprised in the inner stator can provide auxiliary radial suspension force, which can increase the radial load capacity, and also reduce the power consumption for suspension. The basic topology, operation principle, control method, and electromagnetic characteristics were all analyzed. Compared with double stator bearingless switched reluctance motor (DSBSRM), the results of finite element analysis method (FEM) verified that the capacity and stability of radial suspension force are both improved.

INDEX TERMS Switched reluctance motor, bearingless motor, double-stator, radial anti disturbance, wide rotor pole.

I. INTRODUCTION

Flywheel energy storage system is a kind of mechanical battery, which uses the high-speed rotation of flywheel to store energy. The flywheel energy storage system used in vehicle power system, commonly known as "on-board flywheel battery", has the advantages of no noise, no pollution and high energy conversion efficiency compared with internal combustion engine. Compared with the traditional battery, it has the advantages of long service life, high energy density, short charge and discharge time [1].

The motor used in flywheel battery (flywheel motor) is the key component to realize electromechanical energy conversion. In the charging mode, the flywheel motor drives the flywheel to accelerate and stores the electric energy absorbed by the power electronic converter in the form of mechanical energy. In the energy holding mode, the flywheel motor keeps constant speed. In the discharge mode, the flywheel operates

The associate editor coordinating the review of this manuscript and approving it for publication was Qinfen Lu[ID].

as the prime mover to drive the flywheel motor to generate electricity, and converts the mechanical energy stored in the flywheel battery into electrical energy for release. Among the various losses of flywheel energy storage system, the loss of bearing accounts for a large proportion, which can be greatly reduced with the advent of magnetic bearing technology [2].

For the on-board flywheel battery, there exist some technical problems, such as the instability of flywheel rotor caused by on-board working conditions, and the limited volume and mass of flywheel battery under on-board conditions. Electric vehicles need to start, accelerate, go uphill and downhill, brake and stop frequently during driving, especially in urban conditions. With the increase of the complexity of road conditions, the disturbance to the flywheel rotor will be more obvious, which makes the flywheel rotor vulnerable to instability. Therefore, it faces more severe challenges in resisting the disturbance effect to the flywheel rotor and reducing the support energy consumption of flywheel rotor.

Bearingless switched reluctance motor (BSRM) can retain the performance advantages of switched reluctance

motor (SRM) without increasing the motor volume, that is, it has simple rotor structure, strong mechanical robustness and good fault tolerance. BSRM also has the advantages of magnetic bearing, that is, the friction loss caused by traditional mechanical bearing can be eliminated, which is benefit for improving the energy conversion efficiency of flywheel battery. Since there is no need to configure additional radial magnetic bearings, the structure of flywheel battery can be more compact, and the problems of rotor deformation and noise caused by radial magnetic tension imbalance can also solved in BSRM by active radial suspension control. When used as a flywheel motor, it is especially suitable for electric vehicles which has strict requirements on the volume, weight and noise of flywheel battery [3]–[5].

According to the number of winding sets on each stator pole, BSRMs can be divided into two types, that is, double winding bearingless switched reluctance motor (DWBSRM) and single winding bearingless switched reluctance motor (SWBSRM). DWBSRM can be acquired by adding a set of suspension force winding on the stator pole of ordinary SRM, which changes the air gap magnetic field distribution of the motor by controlling the current of the two sets of windings, so as to produce magnetic torque and radial suspension force [6]. SWBSRM generates magnetic torque and radial suspension force by reasonably controlling the winding current on each stator pole. SWBSRM has more universality and practicability because it does not change the structure of the original SRM. At present, SWBSRM has become a research hotspot and development trend in this field [7]–[10]. According to the relative position of rotor and stator, BSRM can also be divided into two types, that is, traditional BSRM with inner rotor and new BSRM with outer rotor structure. When the BSRM with outer rotor is used as a flywheel motor, its rotor can be laminated and encapsulated inside the flywheel, so that the rotor and the flywheel can be combined into one, which is benefit for enhancing the strength of the flywheel rotor, reducing the overall volume and improving the dynamic characteristics and stability of the whole flywheel system.

In order to realize the decoupling of magnetic torque and suspension force in BSRM, scholars at home and abroad tried to study some new types of motor topology [11]–[26]. A single winding hybrid rotor bearingless switched reluctance motor (HRBSRM) was proposed in document [11], whose rotor was composed of annular laminations and fan laminations in the axial direction. The 4-pole windings in radial x and y axis directions were excited separately, and the other 4-pole windings were divided into two phases to conduct in turn. The annular lamination part enhanced the radial load capacity of the hybrid rotor at the non-coincidence position of stator and rotor poles, but made the complexity of magnetic field topology increased, and there still existed a large coupling between torque and suspension force. Reference [13] studied an asymmetry bearingless switched reluctance motor (ABSRM), in which the suspension force ripple is obvious

with the change of rotor position in a full-period. Based on reference [13], a hybrid excitation outer rotor bearingless flywheel motor was studied [14], which exhibits the advantages of high integration and low loss due to outer rotor direct-drive technologies. Reference [15] studied a decoupling control method for 6/2 pole hybrid rotor bearingless switched reluctance motor. Its suspension control was similar to magnetic bearing, with less power switches and low controller cost.

A 8/10 hybrid stator bearingless switched reluctance motor (HSBSRM) which has unequal width stator pole structure was proposed in documents [16] and [17]. The rotation function is provided by the torque windings on four narrow stator poles, and the suspension function is provided by the suspension windings on four wide stator poles. The overlapping area of the suspension pole and the rotor pole is the same, which makes the magnetic conductivity of the suspension winding a constant value and does not change with the rotor position. When the suspension windings conduct, there is no electromagnetic torque output, and the decoupling control of torque and suspension force is realized. Based on the motor structure described in documents [16] and [17], a 12/14 pole hybrid stator bearingless switched reluctance motor (HSBSRM) was proposed in document [18]. The magnetic circuit of HSBSRM becomes shorter, which can strengthen the decoupling and reduce the iron loss.

Reference [19], [20] studied the double stator bearingless switched reluctance motor (DSBSRM). The magnetic flux paths of the main winding and the suspension force winding were independent of each other, which could effectively overcome the coupling effect between these two sets of windings, but the difficulty of system assembly increased. Based on DSBSRM, a permanent magnet was embedded into the inner stator along the axial direction to provide the bias magnetic field required by the radial suspension force to reduce the levitation power consumption, but the structural complexity and processing difficulty of the motor increased [21].

In addition, the literature [22]–[24] has also studied and explored the bearingless switched reluctance motor from various aspects. Literature [23], [24] studied the conical bearingless switched reluctance motor, which reduces the number of stator and rotor, and correspondingly reduced the resources of current sensors, power devices and controllers. However, the coupling between windings was serious and complex, and the difficulty of modeling and control system design increased.

Based on DSBSRM, a new radial-anti-disturbance bearingless switched reluctance motor (RADBSRM) is proposed and studied in this paper, which can overcome the coupling between electromagnetic torque and suspension force, enhance the radial load capacity and anti-disturbance capacity, and improve the radial suspension performance of the rotor. It has prominent application advantages in vehicle flywheel battery and other occasions that are easily disturbed by road conditions and vehicle speed changes.

## II. TOPOLOGY AND OPERATION PRINCIPLES OF THE RADBSRM

A. TOPOLOGY OF RADBSRM

The topology of the RADBSRM studied in this paper is shown in Fig.1 (a). The motor consists of an outer stator, a rotor and a hybrid inner stator. The inner stator can adopt 4-pole or 8-pole structure; The pole number setting rules of outer stator and rotor are the same as those of conventional SRM. Taking the three-phase 12/8/4 three-salient-pole structure as an example, 12 main winding poles are evenly arranged on the inner wall of the outer stator; Eight rotor poles are evenly arranged on the outer wall of the rotor, and the pole width of the rotor is equal to the pole distance of the main winding poles; The hybrid inner stator is composed of a left core, a right core, and a permanent magnet which is magnetized along the axial direction. There are four auxiliary suspension poles evenly arranged on the outer walls of the left core and right core respectively.

Fig.1 (b) shows the distribution diagram of the main windings. There is a set of main windings on each main winding pole. The main windings are not connected with each other, and the windings on radially opposite four poles form a phase, which can be divided into three phases defined as A, B and C. and the currents are marked as $i_{A1} \sim i_{A4}, i_{B1} \sim i_{B4}$, and $i_{C1} \sim i_{C4}$ respectively.

Fig. 1 (c) shows the distribution diagram of the auxiliary windings. For the iron cores on the left and right sides, a set of auxiliary windings are respectively set on each auxiliary suspension pole, and the auxiliary windings on the four auxiliary suspension poles D1, D2, F1 and F2 are connected in series along the x-axis direction to conduct with current i_{Fx}. The auxiliary windings on the four auxiliary suspension poles E1, E2, G1 and G2 are connected in series along the y-axis direction to conduct with current i_{Fy}.

There are actually four air gaps in RADBSRM. The first air gap between the auxiliary suspension pole and the circular inner wall of the rotor core is recorded as g1; The second air gap between the inner stator slot and the circular inner wall of the rotor core is recorded as g2; The third air gap between the rotor pole and the main winding pole of the outer stator is recorded as g3; The fourth air gap between the rotor pole and the outer stator slot is recorded as g4 (g1 < g2, g3 < g4).g1 affects the maximum value of the phase inductance of the auxiliary winding; g2 affects the minimum value of the phase inductance of the auxiliary winding; g3 affects the maximum value of the phase inductance of the main winding; g4 affects the minimum value of the phase inductance of the main winding. In order to obtain large electromagnetic torque and radial suspension force, the first air gap g1 and the third air gap g3 are required to be as small as possible; However, constrained by the assembly process and processing process, the air gaps cannot be too small. Therefore, it is required that the first air gap g1 and the third air gap g3 of small size BSRMs should generally be less than 0.3mm. In order to improve the output power of the motor, the minimum inductance of the main winding is required to be as small as
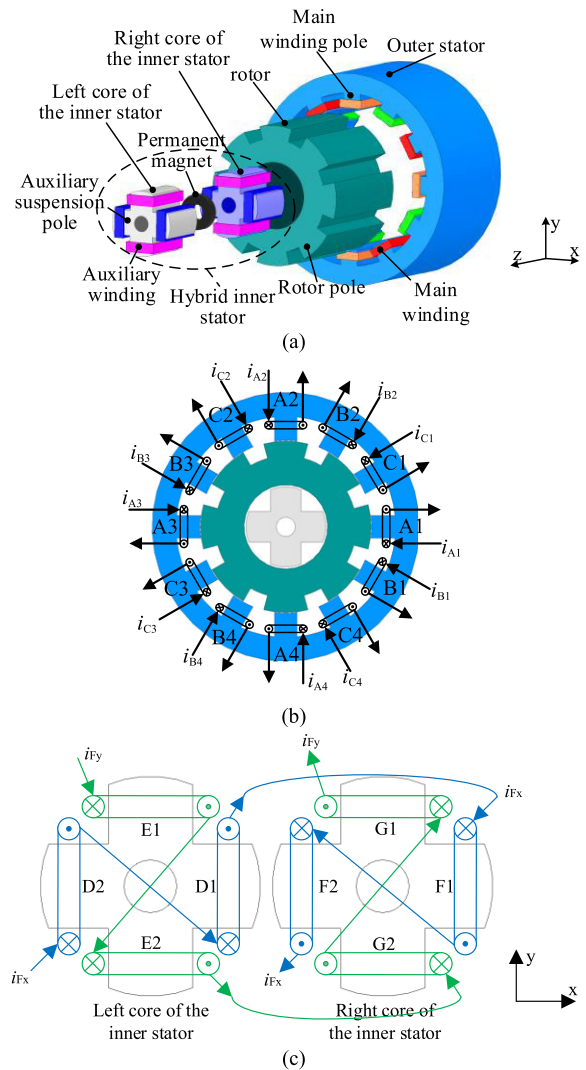
FIGURE 1. Topology of the RADBSRM. (a) Exploded view of structure; (b) Configuration of the main windings on outer stator; (c) Configuration of the auxiliary windings on inner stator.

possible, so the fourth air gap g4 are required to be as large as possible.

B. OPERATING PRINCIPLE OF RADBSRM

The main windings are responsible for generating electromagnetic torque and main suspension force. In the process of rotor rotation, there are always two phases of main windings conducting at the same time. One conducting phase works in the suspension area to provide the main suspension force required for rotor radial suspension by asymmetric excitation, and the suspension area is located in the flat top area of the conducting phase main windings with maximum phase inductance; The other conducting phase works in the torque area to provide the electromagnetic torque required for rotor rotation by symmetrical excitation. The selection of torque phase shall match the operation mode of DSBSRM. If it operates in power-driven mode, the phase with rising inductance

shall be selected as the torque phase. If it operates in power-generation mode, the phase with falling inductance shall be selected as the torque phase.

When the rotor is subjected to serious radial disturbance, in addition to the main suspension force provided by the main windings, the auxiliary windings and permanent magnet can also provide auxiliary suspension force to improve the radial-anti- disturbance performance. The permanent magnet provides the bias magnetic field for the auxiliary suspension force, and the auxiliary windings provides the control magnetic field for the auxiliary suspension force. By adjusting the amplitude and direction of i_{Fx} and i_{Fy}, the auxiliary suspension forces along the x-axis and y-axis can be controlled respectively. The auxiliary suspension force in any direction can be synthesized from the auxiliary suspension forces along the x-axis and y-axis.

Taking the flywheel battery as an example, during the rotation of the motor rotor, the main windings in torque area will conduct with torque current i_{mT} to provide a symmetrical four-pole main flux, which is similar to that of SRM. According to the principle of minimum reluctance, the rotor will move in the direction aligned with the main winding poles under the action of main flux. In energy storage mode, the direction of electromagnetic torque of the main windings is consistent with the rotation direction of the flywheel; In energy release mode, the direction of electromagnetic torque of the main winding is opposite to the driving torque provided by the flywheel, and the mechanical energy stored by the flywheel will be converted into magnetic energy and stored in the magnetic field. When the main switches of the power circuit of the main windings in torque phase are disconnected, its phase current will continue to flow through diodes to release the magnetic energy stored in the magnetic field, and convert the magnetic energy into electrical energy and feed back to the power supply.

III. CONDUCTING RULES AND IMPLEMENTATION OF RADBSRM

A. RADIAL SUSPENSION FORCE DISTRIBUTION STRATEGY

When the rotor is subjected to serious radial disturbance, it is necessary to provide sufficient active suspension force instantaneously in order to quickly restore the rotor to the radial center. Taking the x direction as an example, the expected radial suspension force to be obtained by the rotor is defined as F_x^*; The expected suspension force to be provided by the main windings in suspension area is recorded as F_{mx}^*; The expected auxiliary suspension force to be co-provided by the auxiliary windings and the permanent magnet is recorded as F_{asx}^*.

When $F_x^* \leq F_1$, the required suspension force F_x^* will be provided only the main windings in suspension area.

$$\begin{cases} F_{mx}^* = F_x^* \\ F_{asx}^* = 0 \end{cases} \tag{1}$$

When $F_x^* > F_1$, the required suspension force F_x^* will be co-provided by the main windings in suspension area, the auxiliary windings, and the permanent magnet.

$$\begin{cases} F_{mx}^* = F_1 \\ F_{asx}^* = F_x^* - F_1 \end{cases} \tag{2}$$

Similarly, for the suspension force in y-direction, the radial suspension force expected to be obtained by the rotor is defined as F_y^*; The suspension force expected to be provided by the main windings in suspension area is defined as F_{my}^*; The auxiliary suspension force expected to be co-provided by the auxiliary windings and the permanent magnet is defined as F_{asy}^*.

When $F_y^* \leq F_1$, the required suspension force F_y^* will be provided only by the main windings in suspension area.

$$\begin{cases} F_{my}^* = F_y^* \\ F_{asy}^* = 0 \end{cases} \tag{3}$$

When $F_y^* > F_1$, the required suspension force F_y^* will be co-provided by the main windings in suspension area, the auxiliary windings and the permanent magnet.

$$\begin{cases} F_{my}^* = F_1 \\ F_{asy}^* = F_y^* - F_1 \end{cases} \tag{4}$$

where, F_1 is a critical value determined in the initial design of RADBSRM, which is determined by the structural parameters and winding parameters. When the main suspension force needed to be provided by the main windings is less than the critical value F_1, the main suspension force can be provided more effectively. Otherwise, the efficiency of main suspension force will be reduced due to the influence of magnetic saturation effect.

B. CONDUCTING RULES FOR MAIN WINDINGS

The topological structure of RADBSRM can be regarded as the combination of two special types of switched reluctance motors. One is the SWBSRM with widen rotor poles, and the other is the SWBSRM with annular outer rotor in which a permanent magnet was embedded into the inner stator to provide the bias magnetic field. Therefore, the main windings and the auxiliary windings still have the advantages of small phase to phase mutual inductance, which is a typical merit of SRM.

The self-inductances of three-phase main windings and the two-phase conduction rules of RADBRM are shown in Fig.2, in which the rotor position angle θ is defined as 0° when the main winding poles of phase A are aligned with the adjacent rotor poles. θ is positive when the rotor rotates clockwise, and θ is negative when the rotation direction is opposite. It can be seen that since the pole width of rotor pole is greater than that of the main winding pole, each phase inductance of main windings will form a flat top area, in which the value of phase inductance is the largest, which is called 'inductance flat top area' in this paper. The phase difference of the inductances for

three-phase main windings is 15°, and the inductance period of one phase is 45°.
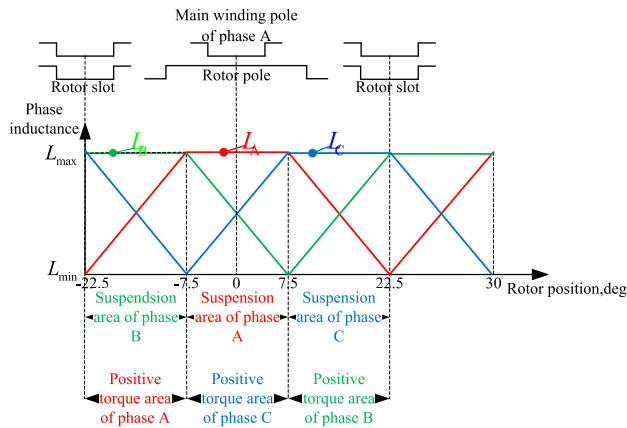

FIGURE 2. Schematic diagram of the conducting rules for main windings.

The specific conduction rules of the main windings are listed in Tab.1. In area 1 ($-22.5° \leq \theta < -7.5°$), the self-inductance of phase B is the largest, so phase B is selected as suspension phase; In area 2 ($-7.5° \leq \theta < 7.5°$), the self-inductance of phase A is the largest, so phase A is selected as suspension phase; In area 3 ($7.5° \leq \theta < 22.5°$), the self-inductance of phase C is the largest, so phase C is selected as suspension phase.

Torque phase shall match the operation mode of RASBARM. Taking area 1 as an example, the self-inductance of phase A gradually increases and the self-inductance of phase C gradually decreases, therefore when RADBSRM operates under power-driven mode, phase A is selected as torque phase, and the current of phase A provides positive electromagnetic torque; When RADBSRM operates under power-generation mode, phase C is selected as torque phase, and the current of phase C provides negative electromagnetic torque to output electric energy. Similarly, the selecting rules of torque phase in area 2 and area 3 can be obtained.

TABLE 1. Conducting rules of main windings.

Operating mode	Area	θ (°)	Suspension phase	Torque phase
Power-driven	1	[-22.5,-7.5]	B	A
	2	[-7.5,7.5]	A	C
	3	[7.5,22.5]	C	B
Power-generation	1	[-22.5,-7.5]	B	C
	2	[-7.5,7.5]	A	B
	3	[7.5,22.5]	C	A

C. IMPLEMENTATION OF RADBSRM

The block diagram of the control system of RADBSRM is shown in Fig.3. Taking the power-driven mode as an example, the rotor position angle θ is detected by the photoelectric sensor, the speed n is calculated according to the change of θ. The expected electromagnetic torque T_e^* is calculated

according to the deviation between the given speed n_{ref} and the actual speed n; The radial displacement signals x and y of the motor rotor along x-axis and y- axis are detected by radial displacement sensors. After comparing x and y with the given radial displacement signals x_{ref} and y_{ref}, the PI controller outputs the expected suspension forces F_x^* and F_y^* according to the radial displacement deviation and then the suspension force distributor distributes the main suspension forces F_{mx}^*, F_{my}^* and auxiliary suspension forces F_{asx}^* and F_{asy}^* according to equations (1)~(4).

The suspension phase and torque phase of main windings are firstly selected by the module 'two-phase-conduction rules of main winding' according to θ, then are sent to the torque/main suspension force controller, and the torque/main suspension force controller calculates the expected main winding currents i_a^*, i_b^* and i_c^* for three phases according to the expected torque T_e^* and main suspension forces F_{mx}^* and F_{my}^*. The auxiliary suspension force controller calculates the expected auxiliary winding currents i_{asx}^* and i_{asy}^* according to the expected auxiliary levitation forces F_{asx}^* and F_{asy}^*. Finally, the current hysteresis loop is used to adjust the currents of main windings and auxiliary windings to follow the expected value.
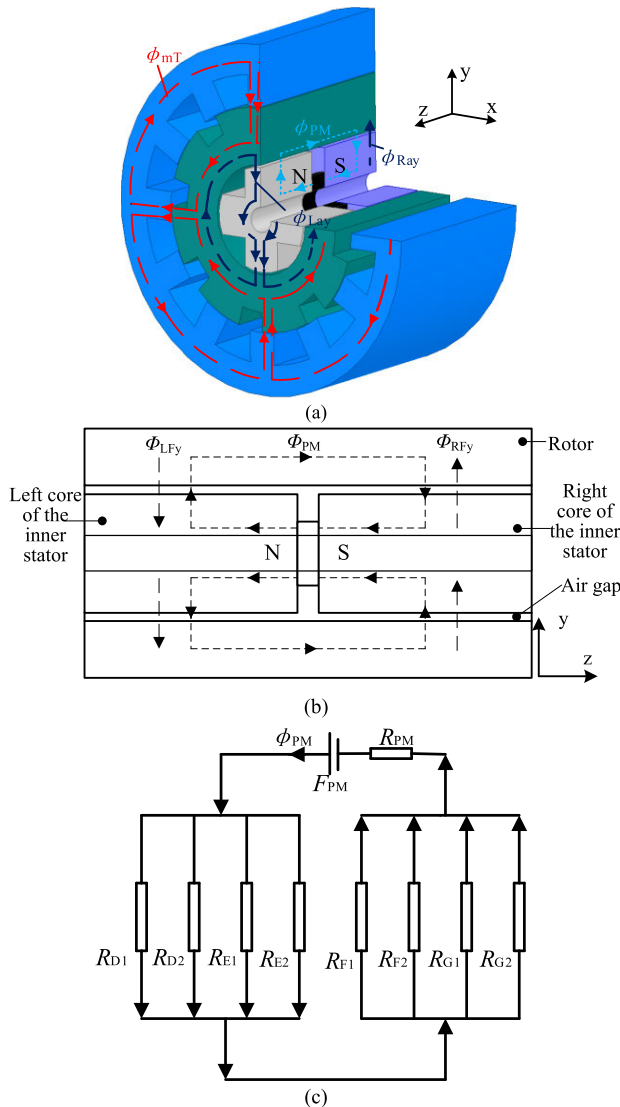
IV. BASIC ELECTROMAGNETIC CHARACTERISTICS ANALYSIS OF RADBSRM
A. FLUX PATHS OF DCBSRM

For the convenience of expression, the current passing through the main windings in suspension area is recorded as i_{mF}, which is called 'suspension current of main winding'. i_{mF} is used to generate the main suspension force. The current passing through the main windings in torque area is recorded as i_{mT}, which is called 'torque current of main winding'. i_{mT} is used to generate electromagnetic torque. Fig.4(a) shows a schematic diagram of the total flux path, where Φ_{mT} represents the magnetic flux generated by i_{mT}; Φ_{PM} represents the bias flux generated by the permanent magnet; Φ_{Fy} represents the control magnetic flux generated by i_{Fy} (in order to distinguish the direction, the control magnetic fluxes in the left inner stator core and the right inner stator core are separately recorded as Φ_{LFy}, Φ_{RFy}). It can be seen that Φ_{mT} is a four-pole flux, which forms a complete flux path through the outer stator core, the third air gap and the rotor core; Φ_{LFy} is a two-pole flux, which forms a complete flux path through the inner stator core, the first air gap and the rotor core. When the thickness of the rotor yoke meets the requirements, the flux paths of the main windings and the auxiliary windings do not intersect, so there is no strong coupling. It should be noted that the magnetic flux Φ_{mF} generated by i_{mF} is omitted in Fig.4(a), and Φ_{mF} also passes through the outer stator core, the third air gap and the rotor core.

In order to explain the generation principle of auxiliary suspension force more clearly, the flux path of permanent magnet is given in Fig.4(b). It can be seen that after passing through the axial magnetic circuit, Φ_{PM} passes through the

FIGURE 3. Block diagram of the RADBSRM control system.

inner stator core, the first air gap and the rotor core to form a complete magnetic flux path. Fig.4(b) also shows the direction of auxiliary suspension force control flux Φ_{LFy}, Φ_{RFy}. The auxiliary suspension force control fluxes along x-axis direction are omitted. Current Φ_{LFy}, Φ_{RFy} can make the magnetic density of the first air gap in positive y-axis direction weakened, while the magnetic density of the first air gap along the negative y-axis direction strengthened, so an auxiliary suspension force pointing to negative y-axis direction will be generated. The auxiliary suspension force is essentially a magnetic tensile stress pointing to the side where the magnetic field is enhanced, that is, Maxwell force.

Fig.4(c) is the simplified magnetic circuit diagram of Φ_{PM}, in which F_{PM} is the equivalent magnetomotive force of permanent magnet, R_{PM} is the magnetoresistance of permanent magnet, $R_{D1} \sim R_{D2}$ and $R_{E1} \sim R_{E2}$ are the air gap magnetoresistances under the auxiliary suspension poles D1 $\sim$ D2 and E1 $\sim$ E2 of the left inner stator respectively; $R_{F1} \sim R_{F2}$ and $R_{G1} \sim R_{G2}$ are the air gap magnetoresistances under the auxiliary suspension poles F1 $\sim$ F2 and G1 $\sim$ G2 of the right inner stator respectively.

B. INDUCTANCE CHARACTERISTICS

The finite element analysis model of RADBSRM is established by ANSYS 20/ Maxwell 3D. The main parameters are shown in Table 2.

In order to illustrate the inductance characteristics of RADBSRM, the transient electromagnetic analysis is carried out by using the finite element model, and the phase inductances of the main windings in RADBSRM and DSBSRM are obtained. The comparison curves are shown in Fig.5. The parameters of DSBSRM are the same with RADBSRM, except that the inner stator structure is different. The windings

TABLE 2. Main parameters of RADBSRM.

Parameter	Value
Outer diameter of the outer stator[mm]	112
Inner diameter of the outer stator[mm]	72
Yoke height of the outer stator[mm]	10
Outer diameter of the rotor[mm]	71.4
Inner diameter of the rotor[mm]	35
Yoke height of the rotor[mm]	12.5
Outer diameter of the inner stator[mm]	34.4
Yoke height of the inner stator[mm]	5
Axial length of rotor and outer stator[mm]	63
Axial length of permanent magnet[mm]	7
Average air gap length[mm]	0.3
Core material	DW310-35
Permanent magnet material	NdFe35
Main winding turns	45
Auxiliary winding turns	18
Outer stator pole arc[deg]	15
Rotor pole arc[deg]	30
Inner stator pole arc[deg]	45

on the outer stator and inner stator of DSBSRM are also called main winding and auxiliary winding respectively. The excitation currents of the main windings of these two motors are also the same. L_A, L_B and L_C are the main winding inductances of phase A, B and C respectively.

(a)

(b)

(c)

FIGURE 4. Flux path diagram. (a) The whole flux paths; (b) The bias flux path of permanent magnet; (c) Simplified bias flux path of permanent magnet.

For RADBSRM, taking LA as an example, it gradually increases from the minimum value to the maximum value in area 1, then remains the maximum value in area 2, and gradually decreases to the minimum value in area 3. Compared with DSBSRM, since the rotor poles of RADBSRM are widened, there exists an inductance flat top area in LA, LB and LC respectively, which makes it possible to generate a sufficiently stable main suspension force from imF of each phase. Lx is the phase inductance of the auxiliary windings on the four auxiliary suspension poles located in x-axis direction. Since the alignment area of the auxiliary suspension pole and the rotor is the same, the Lx of DSBSRM is stable at 0.96mh, while under the influence of bias flux, the Lx of RADBSRM is larger and its value is stable around 2.27mh.

C. SUSPENSION FORCE CHARACTERISTICS

In DSBSRM, the auxiliary windings on inner stator are responsible for generating radial suspension force. Fig.6(a)
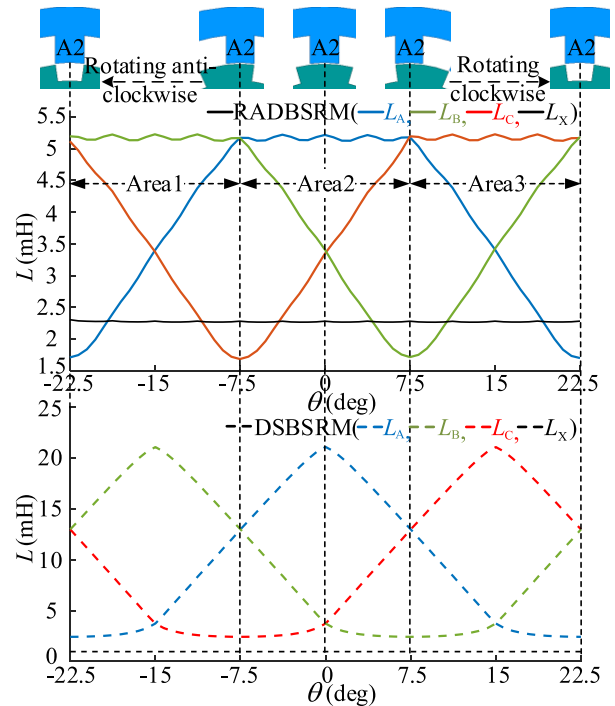
FIGURE 5. Inductance curves of RADBSRM and DSBSRM.

shows the suspension force curves of DSBSRM. It can be seen that when the current i_{yp} of the inner stator winding located in positive y-axis direction increases from 0A to 2.5A, the average value of radial suspension force F_y increases from 0N to 5.77N, and F_y fluctuates only minimally with the change of rotor position angle.

In RADBSRM, the auxiliary winding are responsible for controlling the auxiliary suspension force. Fig.6(b) shows the auxiliary suspension force curves of RADBSRM. When $i_{Fy} = 2.5A$, the average auxiliary suspension force F_{ay} along positive y-axis direction is 36.18N, which is much greater than the suspension force in DSBSRM. RADBSRM can generate suspension force more effectively than DSBSRM, because the permanent magnet can provide bias flux for auxiliary suspension force.

Fig.6 (c) shows the main suspension force F_{my} generated by i_{A2} in RADBSRM when the rotor is in area 1 as shown in Tab.1. When i_{A2} increases from 0A to 2.5A, F_{my} increases from 0N to 41.88N. In RADBSRM, the main suspension force and auxiliary suspension force can be standby and complementary to each other, which is benefit for improving the radical anti-interference ability and radial load capacity of the motor.

D. ELECTROMAGNETIC TORQUE CHARACTERISTICS

Fig.7 shows the electromagnetic torque T_e generated by the main windings of phase C in one inductance cycle in RADBSRM and DSBSRM. It can be seen that T_e increases with the increment of i_c. In the area where the inductance of phase C rises, T_e is positive; In the area where the inductance of phase C drops, T_e is negative. If the main windings of
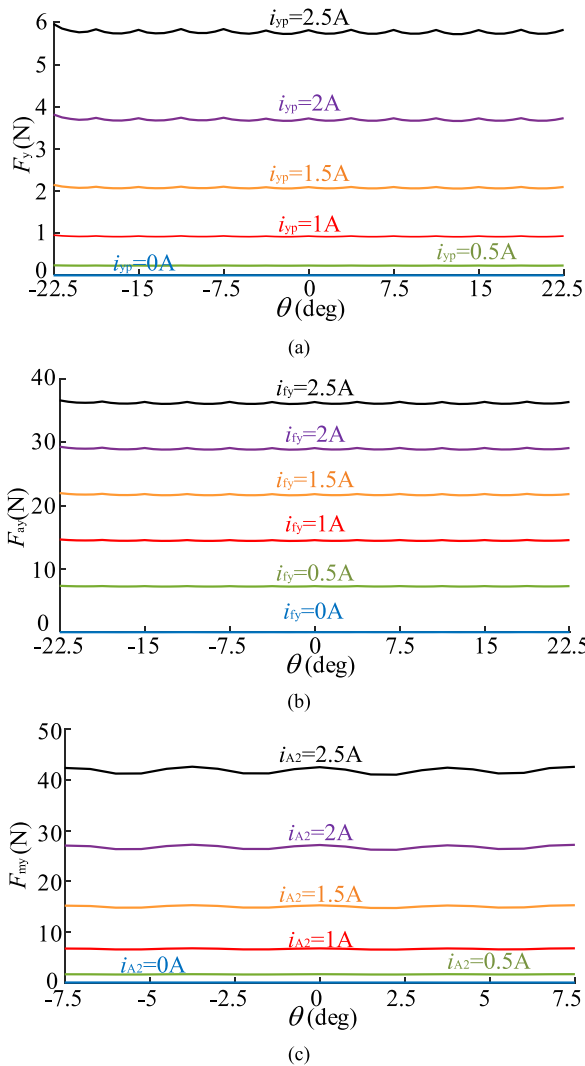
FIGURE 6. Comparison of suspension force between DARBSRM and RADBSRM. (a) The suspension force along y-axis direction in DSBSRM; (b) The auxiliary suspension force along y-axis direction in RADBSRM; (c) The main suspension force along y-axis direction in RADBSRM.

DSBSRM also adopts the two-phase-conduction decoupling strategy, in area 2, only phase A can be selected as the suspension phase (the mean value of electromagnetic torque generated is 0N). When DSBSRM operates in power-driven mode, phase C should be selected as the torque phase (but it cannot effectively generate electromagnetic torque within the range [−7.5°,0°]). Therefore, RADBSRM has more advantages of two-phase-conduction decoupling control of main windings than DSBSRM.

V. DECOUPLING ANALYSIS
Further, the coupling characteristics of RADBSRM are analyzed, which can be the basis for control system design.

A. DECOUPLING OF FLUX PATHS FOR MAIN WINDINGS AND AUXILIARY WINDINGS
Fig.8 shows the distribution curves of gap magnetic densities, in which 0°, 90°, 180° and 270° on the transverse
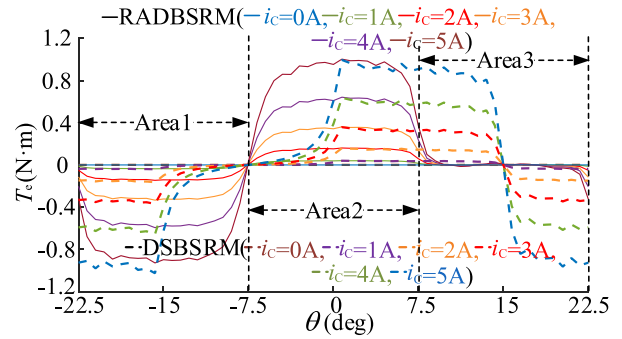
FIGURE 7. Comparison of torque between DSBSRM and RADBSRM.

axis represent the air gaps in positive x-axis, positive y-axis, negative x-axis and negative y-axis direction respectively. Fig.8(a) and Fig.8(b) show the air gap magnetic density distribution under the condition that only auxiliary windings conduct, where $i_{Fx} = 0$ A. When $i_{Fy} = 0$A, Fig.8(a) and Fig.8 (b) show the air gap magnetic density caused by the permanent magnet. It can be seen from Fig.8(a) that the bias flux provided by the permanent magnet PM is evenly and symmetrically distributed, and the air gap magnetic density near each auxiliary suspension pole is about 0.52T. When $i_{Fy} = 2.5$A is applied to the auxiliary winding in y-axis direction, the air gap magnetic density near the auxiliary suspension poles E1 and G1 decreases to 0.26T, while the air gap magnetic density near the auxiliary suspension poles E2 and G2 increases to 0.78T. As can be seen from Fig.8(b), the air gap flux density fluctuation near the main winding poles can be ignored compared with that near the auxiliary suspension poles.

Fig.8(c) and 8(d) show the air gap magnetic density distribution under the condition that only the main windings conduct. Taking the asymmetric excitation of phase A as an example, when i_{A2} changes from 0A to 2.5A, the air gap magnetic density near A2 pole changes from 0 to 318.55mT. Under different values of i_{A2}, the air gap magnetic density near the auxiliary suspension poles changes little, and the magnetic density of the first and second air gaps is approximately uniformly and symmetrically distributed, which verifies that there is good decoupling between the inner stator and the outer stator.

B. DECOUPLING OF MAGNETIC TORQUE AND SUSPENSION FORCE
The results of the electromagnetic torque and main suspension force of main windings calculated by Maxwell 3D are shown in Fig.10. As shown in Fig.9(a), when the main windings in torque phase are symmetrically excited (taking the torque current i_C as an example) with the current increasing from 0A to 5A, the average electromagnetic torque $T_{e(avg)}$ gradually increases from 0 to 0.8 N ·m; When the main windings in suspension phase are asymmetrically excited (taking the suspension current i_{A2} as an example) with the
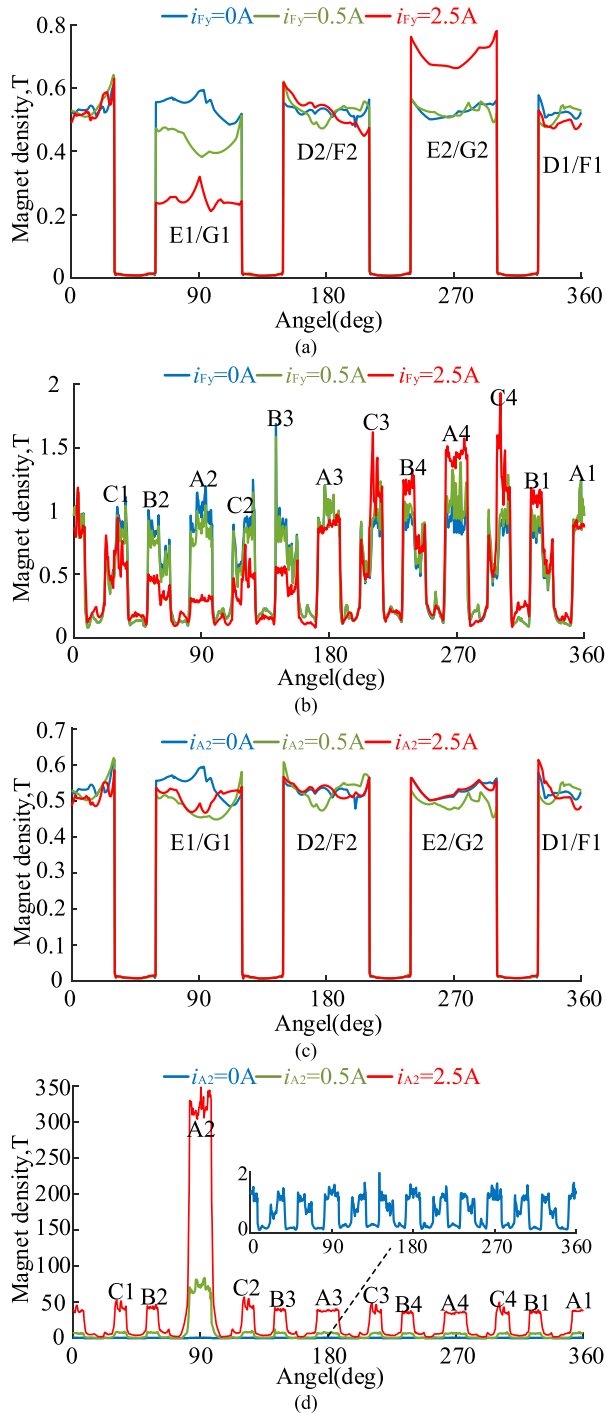
FIGURE 8. Air gap flux density distribution (a) Flux density distribution of air gap g1 and g2 (the main winding is not conducted); (b) Flux density distribution of air gap g3 and g4 (the main winding is not conducted); (c) Flux density distribution of air gap g1 and g2 (the auxiliary winding is not conducted); (d) Flux density distribution of air gap g3 and g4 (the auxiliary is not conducted).

current increasing from 0A to 2.5A, $T_{e(avg)}$ is hardly affected. i_{Fx} (A) $F_{my(avg)}$ (N).

As shown in Fig.9(b), when the torque current i_{mT} remains 0A and the main suspension current i_{A2} increases from 0A to 2.5A, the average suspension force $F_{my(avg)}$ in y-axis

direction increases from 0N to 41.88N; When the main suspension current i_{A2} is 2.5A and the torque current i_C increases from 0A to 5A, $F_{my(avg)}$ increases from 41.88N to 44.37N, with an increament of 5.95%. i_{mT} has a weak coupling effect on main suspension force which can be approximately ignored. In application, this coupling can be further reduced by adjusting the switching angle.
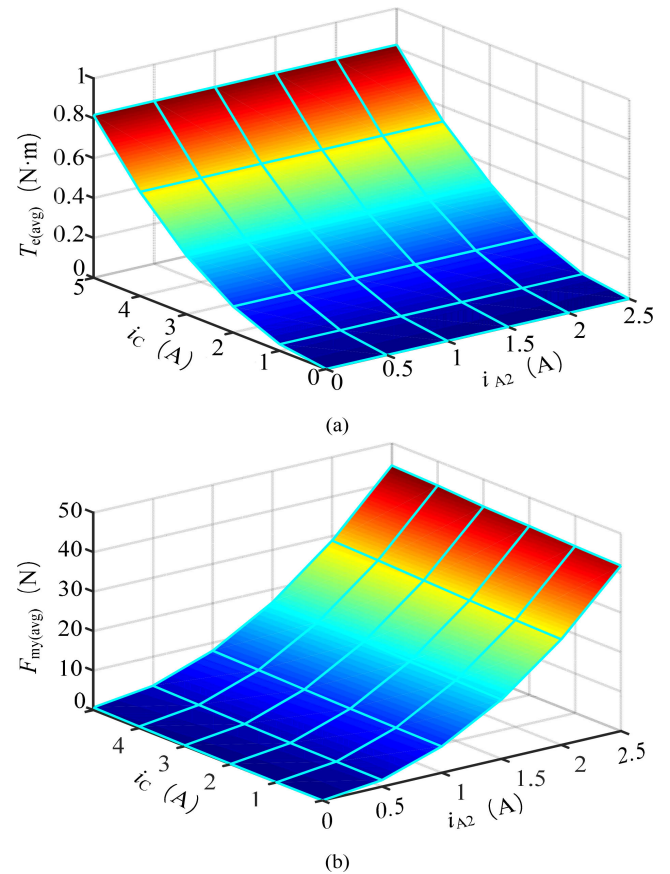
FIGURE 9. Decoupling characteristics of torque and main suspension subsystem. (a) Analysis of coupling influence of main suspension current on torque subsystem; (b) Analysis of coupling influence of torque current on the main suspension subsystem.

As shown in Fig.10(a), when the suspension current of the main winding is 0A and the auxiliary winding current i_{Fx} increases from 0A to -2.5A, the average auxiliary suspension force $F_{ax(avg)}$ in x-axis direction increases from 0N to 36.18N; When i_{Fx} remains -2.5A and the main winding suspension current i_{A2} increases from 0A to 2.5A, $F_{ax(avg)}$ is almost unchanged. As can be seen from Fig.10(b), the auxiliary winding current i_{Fx} also has little effect on the average main suspension force $F_{my(avg)}$ in y-axis direction. When i_{A2} is 2.5A, $F_{my(avg)}$ is almost stable at 41.88N. Therefore, there is good decoupling between the main suspension subsystem and the auxiliary suspension subsystem.

As shown in Fig.11(a), when the auxiliary winding current is 0A and the torque current i_C increases from 0A to 5A, the average electromagnetic torque $T_{e(avg)}$ increases from 0 N·m to 0.82 N·m; When the auxiliary winding current i_{Fy} increases
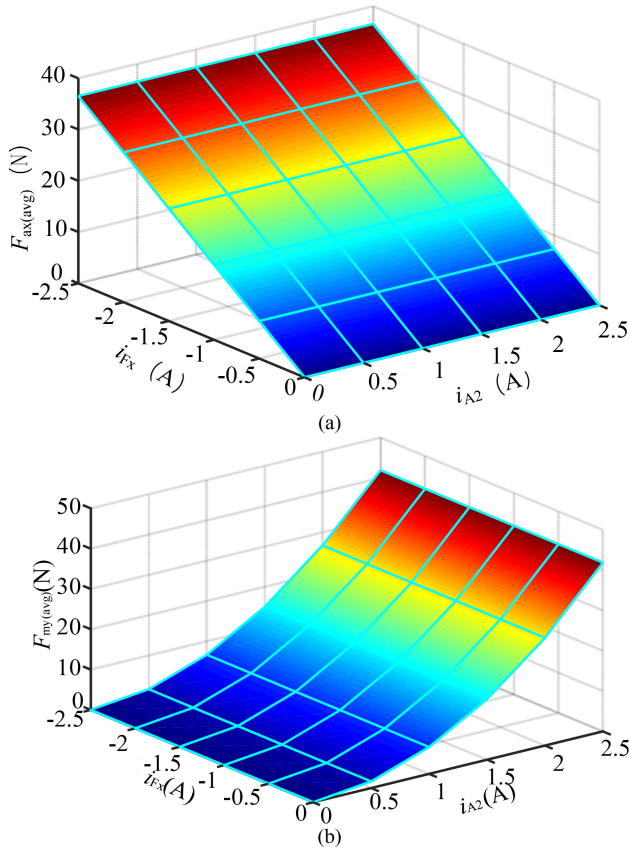
FIGURE 10. Decoupling characteristics of main suspension and auxiliary suspension subsystem. (a) Analysis of coupling influence of main suspension current on auxiliary suspension subsystem; (b) Analysis of coupling influence of auxiliary suspension current on main suspension subsystem.
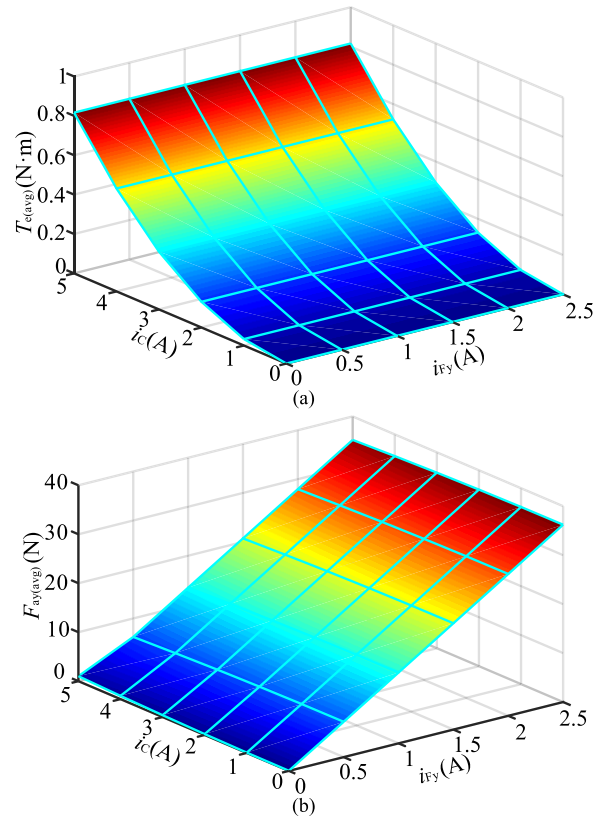

FIGURE 11. Decoupling characteristics of torque and auxiliary suspension subsystem. (a) Analysis of coupling influence of auxiliary suspension current on torque subsystem; (b) Analysis of coupling influence of torque current on auxiliary suspension subsystem.

from 0A to 2.5A, the effect on $T_{e(avg)}$ is very weak. As shown in Fig.11(b), the torque current i_C also has little effect on the average suspension force $F_{ay(avg)}$ in y-axis. When i_{Fy} is 2.5A, $F_{ay(avg)}$ is almost stable at 36.18N, so there is good decoupling between the torque subsystem and the auxiliary suspension subsystem.

VI. PERFORMANCE COMPARISON

The characteristics the new RADBSRM are furthly compared with other typical BSRMs in this section.

In traditional 12/8 DWBSRM, each stator pole is wound with two sets of windings. In addition to the electromagnetic torque, the main windings are also used to provide the bias flux for suspension force. The suspension windings can provide the control flux for suspension force. By superimposing these two kinds of flux, the suspension force can be generated. BSRM is a nonlinear and strongly coupled complex system. It is difficult to realize the decoupling control of electromagnetic torque and suspension force in practice.

Compared with DWBSRM, the manufacturing cost of SWBSRM can be reduced, and the power can be furtherly improved. The structure of SWBSRM is the same as that of ordinary SRM. The coils on each stator pole are disconnected

from each other and controlled independently. By changing the current in the winding, the flux density under the stator pole can be changed, therefore the required electromagnetic torque and radial force can be produced simultaneously.

In HRBSRM, the stator structure is consistent with that of SRM, while the rotor is different. The fan laminations provides suspension force, while the annular laminations not only provide electromagnetic torque but also provides suspension force. The control strategy is easy to implement, but its axial length is extended, which is not conducive to improving the critical speed or power density.

Compared with the 8/10 HSBSRM, the 12/14 HSBSRM has shorter magnetic circuit, which can strengthen the decoupling and reduce the iron loss.

In DSBSRM, the torque control is the same as 12/8 SRM, and the required suspension force can be controlled by controlling the winding current on the inner stator. Decoupling control can be realized by maintaining a certain thickness of the rotor yoke during machining, but the machining requirements are high.
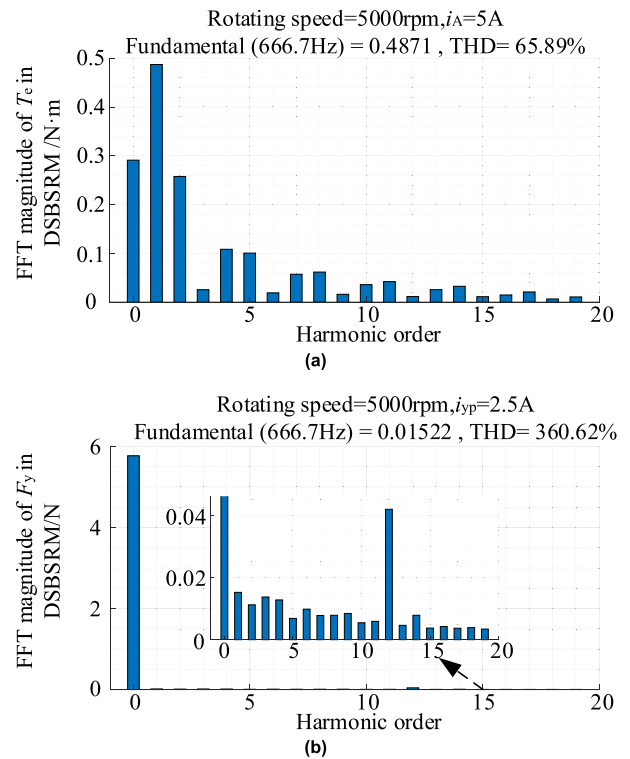
In RADBSRM, the radial load capacity and anti-disturbance ability can be enhanced, and the power consumption for radial suspension can be reduced due to the permanent magnet comprised in the inner stator.
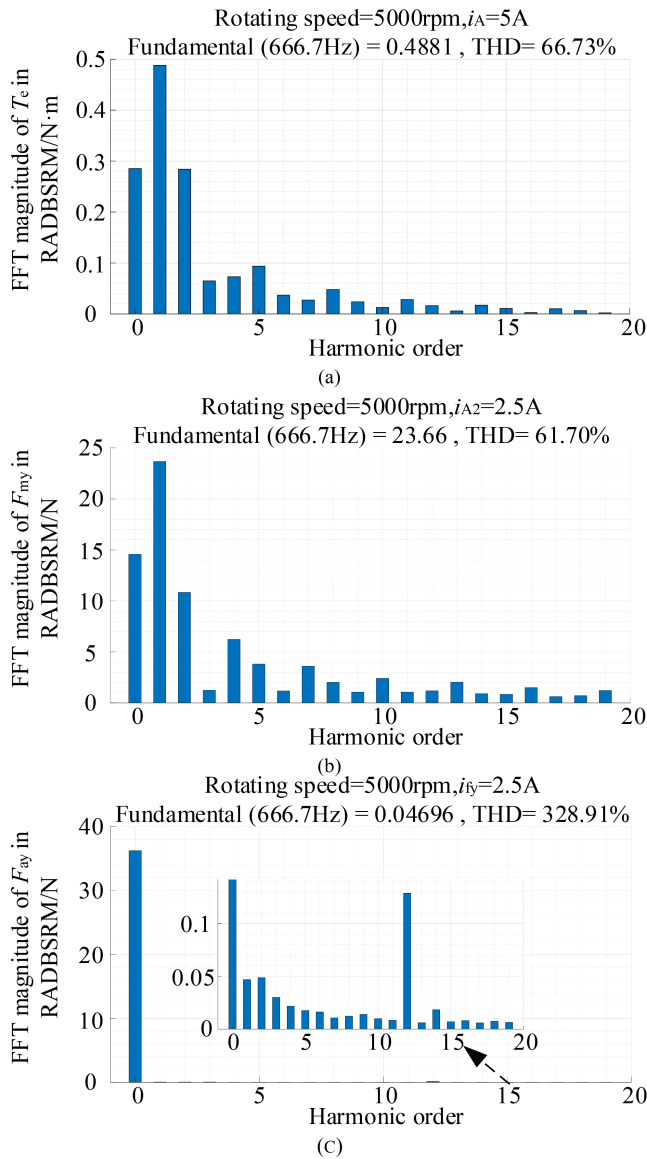
FIGURE 12. Harmonic analysis results of RADBSRM. (a) FFT results of electromagnetic torque; (b) FFT results of main suspension force; (c) FFT results of auxiliary suspension force.

FIGURE 13. Harmonic analysis results of DSBSRM. (a) FFT results of electromagnetic torque; (b) FFT results of suspension force.

Since there is still no clear comparative data about the efficiency, power factor, harmonic and other indicators of various types of BSRMs available in the published literatures, therefore Maxwell 3D is used to establish the models of several typical BSRMs for preliminary performance comparison in this paper. The main physical dimensions, winding parameters and excitation current of these motors are the same.

The electromagnetic torque, main suspension force and auxiliary suspension force of RADBSRM are analyzed by FFT (fast Fourier transform). The rotor speed is 5000rpm, therefore the fundamental frequency is 667Hz. The results are shown in Figure 12. It can be seen that T_e, F_{my} and F_{ay} contain large DC components. The total harmonic distortion (THD) of T_e, F_{my} and F_{ay} is 66.73%, 61.70% and

328.91% separately. One reason for the large THD value is that the DC component is included in THD, especially for F_{ay}. But the DC component does not cause stator vibration, and even contributes greatly to the average value. The amplitude of the second order harmonic of T_e and F_{my}, and the amplitude of the twelfth order harmonic of F_{ay} are large, which may cause large vibration response of stator. The reason for large harmonics is the use of square wave current control method, which is a major problem of switched reluctance motor, and can be suppressed by structural optimization and control strategy [25], [26].

DSBSRM has the most similar structure to RADBSRM, so the FFT results of electromagnetic torque and suspension force for DSBSRM are given in Figure 13 for comparison. It can be seen that the DC component of T_e is the same as that of RADBSRM, and the harmonic of torque T_e similar to that of RADBSRM. The THD of the suspension force F_y is greater than the main suspension force F_{my} of RADBSRM, and the DC component of F_y is less than that of F_{my}, which indicate that the harmonic content of RADBSRM is better than that of DSBSRM, and the suspension ability of RADBSRM is stronger than that of DSBSRM.

Table 3 shows the comparison of some performance parameters of concern, in which the excitation currents are listed simultaneously. The RADBSRM has not been optimized with multiple objectives in system level, therefore the performance parameters are not the optimal value that the RADBSRM can achieve. Considering that DWBSRM is a

TABLE 3. Main parameters of RADBSRM.

Performance parameter	DWBSRM [27]	SWBSRM	DSBSRM	RADBSRM
Main suspension efficiency [N/W]	5.04	5.2877 (i_{A2}=7.5A, i_{A4}=7.5A, i_{A1}=5A i_{A3}=5A)	7.9041 (i_{yp}=2.5A)	18.3684 (i_{A2}=2.5A)
Auxiliary suspension efficiency [N/W]	/	/	/	19.1693 (i_{Fy}=2.5A)
THD of main suspension force	/	89.86%	360.62% (i_{yp}=2.5A)	61.70% (i_{A2}=2.5A) (i_{Fy}=2.5A)
THD of auxiliary suspension force	/	/	/	328.91% (i_{Fy}=2.5A)
Electromagnetic torque efficiency [Nm/W]	0.011	0.0316 (i_A=5A)	0.0113 (i_A=5A)	0.0225 (i_A=5A)
THD of electromagnetic torque	/	65.46% (i_A=5A)	65.89% (i_A=5A)	66.73% (i_A=5A)

traditional type of BSRM, and the performance advantages of other typical types of BSRMs relative to DWBSRM have been widely analyzed and described. Therefore, a finite element analysis model is no longer reestablished for analysis, but only the data of references are cited [27]. It can be seen that the suspension efficiency, electromagnetic torque efficiency, THD of suspension force, THD of electromagnetic torque of the proposed RADBSRM are better than others types of BSRMs (including DWBSRM, SWBARM, DSBSRM).

VII. CONCLUSION

A new type of radial-anti-disturbance bearingless switched reluctance motor is proposed in this paper. The topology, operation principle and control strategy are described. Its electromagnetic and decoupling characteristics are analyzed and verified by finite element method. RADBSRM has the following excellent performance.

(1) The radial load capacity and anti-disturbance ability are enhanced. Specifically, the main windings can provide electromagnetic torque and main suspension force simultaneously. When the rotor is seriously disturbed in radial direction, the auxiliary windings and the permanent magnet can also co-provide auxiliary suspension force to make the rotor quickly restore to the radial center.

(2) The coupling between electromagnetic torque and radial suspension force are effectively weakened. Specifically, the flux paths of the main windings and the auxiliary windings are not interconnected, so the coupling between the electromagnetic torque and the auxiliary suspension force can be effectively weakened structurally. The inductance change rate of the auxiliary windings in each phase and the main windings in suspension area are all approximately to zero with respect to the rotor position angle, which will not generate electromagnetic torque after excitation.

(3) The power consumption for radial suspension is reduced. Because the permanent magnet comprised in the inner stator can provide constant bias flux for the auxiliary suspension force, the magnitude and direction of the auxiliary suspension force can be controlled by adjusting the auxiliary winding current, and the auxiliary windings can generate the suspension force more effectively than DSBSRM.

As a high-precision finite element simulation software, ANSYS can analyze the electromagnetic characteristics of motor and simulate its control effect in combination with external circuit. Therefore, it is often used for rapid verification of new structure motor [28]. In this paper, the excellent performance of RADBSRM is analyzed by ANSYS, and the feasibility of the proposed scheme is preliminarily verified, which lays a foundation for subsequent research. The actual operation test needs to establish a complete experimental control system, which involves a lot of work such as prototype processing, control strategy optimization, controller design and debugging, and needs to be further carried out by the research group.

REFERENCES

[1] Y. Tang and H. Zhu, "Development and key technologies of flywheel energy storage system for vehicle," *Electr. Mach. Control Appl.*, vol. 43, no. 5, pp. 38–46, 2016.

[2] H. Zhu and Y. Tang, "Key technologies and application trends of flywheel energy storage system," *Machinery Des. Manuf.*, vol. 311, no. 1, pp. 265–268, 2017.

[3] J. Zhang, H. Wang, L. Chen, C. Tan, and Y. Wang, "Multi-objective optimal design of bearingless switched reluctance motor based on multi-objective genetic particle swarm optimizer," *IEEE Trans. Magn.*, vol. 54, no. 1, pp. 1–13, Jan. 2017.

[4] J. Zhang, H. Wang, S. Zhu, C. Tan, and Y. Wang, "Multi-objective optimization of current waveform of bearingless switched reluctance motor for torque ripple and radial force ripple reduction," in *Proc. 14th IEEE Conf. Ind. Electron. Appl. (ICIEA)*, Jun. 2019, pp. 424–428.

[5] Y. Zhou, Y. Sun, and Z. Wang, "A double-stator bearingless switched reluctance motor drive control system for flywheel energy storage," *Proc. CSEE*, vol. 35, no. 21, pp. 5600–5606, 2015.

[6] Q. Yu and X. Cao, "Hysteresis control of torque and levitation force for dual-winding bearingless switched reluctance motor," in *Proc. 14th IEEE Conf. Ind. Electron. Appl. (ICIEA)*, Xi'an, China, Jun. 2019, pp. 1173–1178.

[7] X. Cao, H. Yang, L. Zhang, and Z. Deng, "Compensation strategy of levitation forces for single-winding bearingless switched reluctance motor with one winding total short circuited," *IEEE Trans. Ind. Electron.*, vol. 63, no. 9, pp. 5534–5546, Sep. 2016.

[8] X. Cao, H. Yang, Z. Deng, and L. Zhao, "Equivalent transformation and control for single-winding bearingless switched reluctance motors," *Electr. Power Compon. Syst.*, vol. 44, no. 9, pp. 1040–1050, May 2016.

[9] P. Liu and X. Cao, "Control method for single-winding 12/4 bearingless switched reluctance motor," in *Proc. 14th IEEE Conf. Ind. Electron. Appl. (ICIEA)*, Xi'an, China, Jun. 2019, pp. 2087–2091.

[10] X. Wu, Y. Yang, and Z. Liu, "Theoretical analysis and simulation of single-winding bearingless switched reluctance generator with wider rotor teeth," *Int. J. Appl. Electromagn. Mech.*, vol. 56, no. 3, pp. 387–398, Feb. 2018.

[11] C. R. Morrison, M. W. Siebert, and E. J. Ho, "Electromagnetic forces in a hybrid magnetic-bearing switched-reluctance motor," *IEEE Trans. Magn.*, vol. 44, no. 12, pp. 4626–4638, Dec. 2008.

[12] C. R. Morrison, "Bearingless switched reluctance motor," U.S. Patent 6 727 618 B1, Apr. 27, 2004.

[13] Y. Yuan, Y. Ma, J. Xu, F. Yang, and K. Xie, "Full-period suspension force accurate modelling for a novel bearingless switched reluctance motor," *Electron. Lett.*, vol. 54, no. 24, pp. 1397–1399, 2018.

[14] F. Yang, Y. Yuan, G. Meng, and L. Yan, "Design and analysis of a high-integration and low-loss bearingless flywheel motor in vehicle," *Electron. Lett.*, vol. 57, no. 10, pp. 390–392, May 2021.

[15] Z. Liu, "A decoupling control method for compound rotor bearingless switched reluctance motor," CHN Patent 2016 11 052 688.3, May 10, 2017.

[16] D.-H. Lee, H. Wang, and J.-W. Ahn, "Modeling and control of novel bearingless switched reluctance motor," in *Proc. IEEE Energy Convers. Congr. Expo.*, San Jose, CA, USA, Sep. 2009, pp. 276–281.

[17] Z. Guan, F. Zhang, and J.-W. Ahn, "High speed direct current compensation control for 8/10 bearingless SRM," in *Proc. IEEE Int. Symp. Ind. Electron.*, Hangzhou, China, May 2012, pp. 1934–1939.

[18] Z. Xu, D. Lee, and J. Ahn, "Suspending force control of a novel 12/14 hybrid stator pole type bearingless SRM," in *Proc. 15th Int. Conf. Electr. Mach. Syst. (ICEMS)*, Sapporo, Japan, 2012, pp. 1–5.

[19] Y. Sun, F. Yang, Y. Yuan, F. Yu, Q. Xiang, and Z. Zhu, "Analysis of a hybrid double stator bearingless switched reluctance motor," *Electron Lett.*, vol. 54, no. 24, pp. 1397–1399, 2018.

[20] Y. Zhou and Y. Sun, "A double-stator type bearingless switched reluctance dual-channel full-period generator," *Proc. CSEE*, vol. 35, no. 9, pp. 2295–2303, May 2015.

[21] Y. Yuan, Y. Ma, S. Guo, F. Yang, and B. Xu, "Suspension performance analysis of a novel bearingless motor," *Electron. Lett.*, vol. 56, no. 3, pp. 132–134, Feb. 2020.

[22] Z. Liu, J. Cai, and Y. Yang, "4-DOF hybrid-structure bearingless switched reluctance motor and its winding optimization design," *Electr. Mach. Control*, vol. 22, no. 6, pp. 49–61, 2018.

[23] C. Liu, X. Cao, X. Li, X. Wang, and Z. Deng, "Current delta control for conical bearingless switched reluctance motors," in *Proc. 13th IEEE Conf. Ind. Electron. Appl. (ICIEA)*, Wuhan, China, May 2018, pp. 2075–2078.

[24] G. Messager and A. Binder, "Observer-based pole placement control for a double conical high-speed bearingless permanent magnet synchronous motor," in *Proc. 18th Eur. Conf. Power Electron. Appl. (EPE ECCE Eur.)*, Karlsruhe, Germany, Sep. 2016, pp. 1–10.

[25] J. Dong, J. W. Jiang, B. Howey, H. Li, B. Bilgin, A. D. Callegaro, and A. Emadi, "Hybrid acoustic noise analysis approach of conventional and mutually coupled switched reluctance motors," *IEEE Trans. Energy Convers.*, vol. 32, no. 3, pp. 1042–1051, Sep. 2017.

[26] R. Matsui, N. Nakao, and K. Akatsu, "Torque/current ratio improvement and vibration reduction of switched reluctance motors using multi-stage structure," in *Proc. Int. Power Electron. Conf. (IPEC-Hiroshima-ECCE ASIA)*, May 2014, pp. 1128–1134.

[27] Q. Xiang, "Parameter design and operation control of 5-DOF single-winding bearingless switched reluctance motor for flywheel batteries," Ph.D. dissertation, Dept. Elect. Eng., Jiangsu Univ., Zhenjiang, China, 2013.

[28] J. Liu, "Numerical simulation and analysis on electromagnetic field of switched reluctance motor based on ANSYS," M.S. thesis, Dept. Mechtron. Veh. Eng., Chongqing Jiaotong Uni. Chongqing, China, 2015.

YUNHONG ZHOU received the B.S., M.S., and Ph.D. degrees from the School of Electrical Engineering, Jiangsu University, Zhenjiang, China, in 2005, 2010, and 2012, respectively, all in electrical engineering. Since 2012, she has been with the Nanjing Institute of Technology, Nanjing, China, where she is currently an Associate Professor with the School of Power Engineering. She was a Visiting Scholar with Southeast University, Nanjing, from 2019 to 2020. Her research interests include electric drive, flywheel energy storage, and intelligent power distribution technology.

JIAHAO JIANG was born in Nantong, Jiangsu, China, in 1996. He received the B.Sc. degree from the School of Electric Power Engineering, Nanjing Institute of Technology, Nanjing, China, in 2019, where he is currently pursuing the master's degree. His main research interests include characteristic analysis and application of bearingless machines.

YUKUN SUN was born in 1958. He is currently a Professor with the School of Power Engineering, Nanjing Institute of Technology. His research interests include optimal control of special motor, bearingless motors, flywheel energy storage systems, and renewable energy generation.

PAN HU was born in Nanjing, Jiangsu, China, in 1995. He received the B.Sc. degree from the School of Electric Power Engineering, Nanjing Institute of Technology, Nanjing, in 2019, where he is currently pursuing the master's degree. His main research interest includes the design and optimization design of bearingless machines.

• • •